JOURNAL OF CATALYSIS 135, 200–222 (1992)

The Effect of Second-Phase Oxides on the Catalytic Properties of Dispersed Metals: Cobalt Supported on 12% WO_3/Al_2O_3

R. ZHANG,*,[1] J. A. SCHWARZ,*,[2] A. DATYE,† AND J. P. BALTRUS‡

*Department of Chemical Engineering and Materials Science, Syracuse University, Syracuse, New York 13244; †Department of Chemical and Nuclear Engineering, University of New Mexico, Albuquerque, New Mexico 87131; and ‡United States Department of Energy, Pittsburgh Energy Technology Center, Pittsburgh, Pennsylvania 15236

Received May 16, 1991; revised December 3, 1991

The differences in the amphoteric properties of WO_3 and Al_2O_3 were exploited and cobalt precursors were selectively mounted on the tungsten oxide phase of a 12% WO_3/Al_2O_3 composite. Temperature-programmed reduction (TPRd), transmission electron microscopy (TEM), X-ray photoelectron spectroscopy (XPS), and catalyst performance testing using H_2/CO methanation as a test reaction revealed that this composite-supported catalyst's properties were significantly different from cobalt supported on alumina. Cobalt crystallites as well as a $CoAl_2O_4$ type of surface species are formed on the Al_2O_3 support. The presence of WO_3 as a second-phase oxide offers the possibility for a greater number of surface compounds to be formed on the composite. Specifically, cobalt–tungsten interaction species are formed. We provide evidence that strongly suggests the active catalytic center in the conversion of H_2 and CO to methane is a (cobalt–tungsten) interaction species. These active centers are present on Co/WO_3, $Co/12\%\ WO_3/Al_2O_3$, and a commercial cobalt/tungsten oxide compound. A portion of the cobalt in these active centers is not reduced to the metallic state.

INTRODUCTION

Tungsten oxide on an alumina carrier has been studied by a number of techniques. These include Raman spectroscopy (*1, 2*), X-ray absorption near edge spectroscopy (*2*), X-ray photoelectron spectroscopy (*2–4*), UV-visible diffuse reflection spectroscopy (*5, 6*), electron paramagnetic resonance spectroscopy (*7*), and the properties of these composites when suspended in water (*8*). These studies had, as their primary goal, the elucidation of the structural state of the second-phase oxide. Recently, we reported on the effect of WO_3 loading on the surface acidity of WO_3/Al_2O_3 composite oxides (*9*). This study, as well as others from our laboratory, has had as a goal the characterization of these oxidic materials in aqueous environments such as those employed during conventional methods for introducing catalytic metals. Our reasons for this were based on developing a thorough understanding of the surface charge development of these oxides when placed in electrolytes of varying pHs.

The pH at which there is a change in the sign of the surface potential of an oxide is designated the point of zero charge (pzc). At this pH value, there will exist positive, negative, and neutral surface charge carriers; the sum of the first two will result in a net charge of zero. The pzcs of alumina and tungsten oxide are separated by ~5 pH units (*8*). Composite oxides formed from these pure phases provide a model system for designing catalytic structures by varying the preparation procedures and then studying the performance of the resulting supported-metal catalysts.

[1] Scientific Committee of Lanzhou, People's Republic of China.

[2] To whom correspondence should be addressed.

0021-9517/92 $3.00

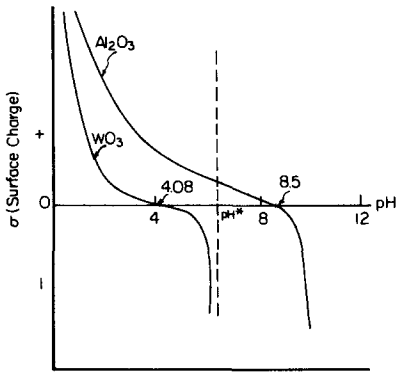

FIG. 1. Schematic depicting the selective metal-support exchange hypothesis. At pH = pH*, the Al_2O_3 phase has a positive charge and WO_3 phase a negative charge.

A pH-directed or selective metal-support exchange exploits the surface charge development on oxides during aqueous impregnation of catalytic precursors. While the thermodynamic properties of these oxides have been reasonably well established, the catalytic properties of a second-phase oxide acting as an anchor for a catalytic metal have not.

The fact that the pzcs of the pure phases are separated by ~5 pH units provides a wide range for adjusting impregnating conditions during catalyst preparation. Figure 1 depicts the strategy of selective metal-support exchange. The differences in the amphoteric behavior of the two components in a composite are exploited resulting in opposite charges on each component's surface. Careful adjustment of the impregnant pH (e.g., pH*) and choosing a suitable precursor, i.e., one whose speciation in the aqueous phase is known, will result in a tungsten oxide phase that is a cation exchanger and an alumina phase that is an anion exchanger. The simplicity of this concept relies on two important conditions that must be met and must be determined experimentally. The first is that the pH-dependent surface charge development of each phase conforms to that of the pure compounds and they develop "charge" independent of the presence of their counterpart. The second is that adsorption of the ionic solute is controlled by surface charge.

The objective of this study is to test the selective metal-support exchange hypothesis *and,* if valid, to evaluate the catalytic performance of a metal mounted on a second-phase oxide. We chose cobalt nitrate as the catalytic precursor because its speciation in the aqueous phase has been reliably established (*10*) and procedures for catalyst activation are available (*11*).

Temperature-programmed reduction (TPRd) data of the dried precursors were obtained subsequent to catalyst impregnation. The calcined catalysts were examined by transmission electron microscopy (TEM) and the catalysts, after reduction, were studied using X-ray photoelectron spectroscopy (XPS). Finally, the catalytic properties of the composite oxide-supported cobalt were determined in relation to that metal's properties when supported on each of the pure phases. Temperature-programmed reaction (TPRx) of CO, steady-state CO hydrogenation, and the carbon inventory subsequent to reaction, as revealed by temperature-programmed surface reaction (TPSR), were the methods employed.

EXPERIMENTAL

MATERIALS

The alumina used in this work was derived from ground (40–80 mesh) $\frac{1}{16}$-in. extrudate, γ phase, obtained from Americn Cyanamid (Lot 85-NA-1402), having a BET surface area of 150 m^2/g and pore volume of 0.48 cc/g. It was treated at 875 K for 24 h before use. The tungsten oxide was 99.7% tungsten trioxide from Alfa, (Lot B021). Tungsten oxide is nonporous (average particle size ~0.04 mm) with a BET surface area of 1 m^2/g. The WO_3 was calcined at 875 K for 24 h before use. The 12% WO_3/Al_2O_3 composite was made by dry impregnation of ammonium metatungstate $[(NH_4)_6H_2W_{12}O_{40} \cdot 5H_2O]$ obtained from GTE Sylvania. The composite oxide was dried at 380 K overnight and calcined at 875

K for 24 h. Its BET area was 131 m^2/g. The point of zero charge of each support was determined by mass titration and the values for Al_2O_3, WO_3, and 12% WO_3/Al_2O_3 were 8.5, 4.08, and 6.08 (*8*). All samples were stored in a dry box purged with N_2.

During the course of this study, we found that having available characterization and performance data from a commercially prepared bulk cobalt–tungsten oxide sample would be useful for interpreting data obtained from the laboratory-prepared catalysts. Alfa products supplied a compound (Lot F10B) that they designated cobalt tungstate. X-ray analysis showed that this was not stoichiometric $CoWO_4$; it was partially amorphous with some crystallinity. After calcination of 875 K for 6 h, X-ray analysis showed that the structure was reformed to $CoWO_4$. The procedures for treatment and results obtained from study of this sample are presented later in the Experimental and then in the Results sections, and a discussion of the relationship of its properties to the dispersed catalysts is presented in the final section of this report.

Catalysts

The catalysts were prepared from a $Co(NO_3)_2 \cdot 6H_2O$ precursor obtained from Fluka Chemicals (Lot 270876). Since equal weight loadings of Co on each support were required, preliminary experiments were conducted, and based on those results catalysts for characterization and performance evaluation were prepared. The preliminary experiments were performed at two levels. Equilibrium adsorption experiments using 2 g of each support and 25 cm^3 of electrolyte (0.027 mol/liter) were conducted. The pH during preparation was maintained at 6. Following these, dry impregnation and pseudo-wet impregnation methods were employed. The conditions for dry impregnation are given in Table 1A. The volume of water used for the WO_3 support was scaled to the mass of WO_3 used based on a water/mass ratio that we used in an earlier study (*8*). The conditions for pseudo-wet impregnation are given in Table 1B. Following their preparation, the solids were filtered and then dried at 380 K for 24 h. The weight loadings on the dried catalysts prepared by both methods were determined by extensive washings of cobalt from the support with 1 *N* H_2SO_4 at a temperature of 340 K followed by AA analysis. The Perkin–Elmer Model 2380 spectrophotometer was calibrated using Alfa products 88060AA standard solution (Lot 051183). Replicate runs demonstrated that our reproducibility was ± 0.04 ppm. Additional samples with loadings of 1 and 3% by weight were prepared by the pseudo-wet impregnation method. The conditions are given in Tables 1C and 1D. Characterization and performance studies were conducted only on those samples prepared by the pseudo-wet impregnation method.

Catalyst Characterization

Apparatus and Procedures

TPRd. The TPRd unit consisted of a gas handling system, a thermal conductivity cell and associated electronics (Fisher Model 1200 gas partitioner), linear temperature programmer (Omega Model CN-2011J), recorder (IBM PC), sample holder, furnace, and cold traps. A complete description of the configuration can be found elsewhere (*12*).

In these experiments, 100 mg of nonactivated and nonpassivated cobalt catalyst was dehydrated in a 100 cm^3/min argon stream by heating from room temperature to 423 K at a heating rate of 5 K/min. The system was held at 423 K for 1 h and cooled to room temperature. After confirming that room-temperature reduction does not occur, the system was switched to an 8.7% H_2 + Ar gas stream with a flow rate of 40 cm^3/min and flushed for 15 min. The system was then heated from room temperature to 773 K at a heating rate of 20 K/min. During the heating process, the hydrogen signal was monitored continuously. The supports themselves showed no H_2 consumption during blank runs.

TABLE 1

Catalyst Preparation

	Volume of deionized water (ml)	$Co(NO_3)_2 \cdot 6H_2O$/g	Support weight (g)	Contact time (min)	pH of precursor solution
		A. Dry impregnation (6%)			
Co/Al_2O_3	5.0	3.04	10.03	5	4.9
$Co/WO_3/Al_2O_3$	5.0	3.03	10.06	5	4.9
Co/WO_3	0.5	3.04	9.99	5	2.0
		B. Pseudo-wet impregnation (6%)			
Co/Al_2O_3	20	11.87	2.04	10	4.9
$Co/WO_3/Al_2O_3$	20	11.84	2.04	10	4.9
Co/WO_3	6.3	38.69	2.03	10	2.0
		C. Pseudo-wet impregnation (3%)			
Co/Al_2O_3	10	2.9	2.01	10	4.9
$Co/WO_3/Al_2O_3$	10	2.9	2.03	10	4.9
Co/WO_3	4.3	10.3	2.05	10	2.9
		D. Pseudo-wet impregnation (1%)			
Co/Al_2O_3	20	1.5	2.0	60	6
$Co/WO_3/Al_2O_3$	20	1.5	2.22	60	6
Co/WO_3	10	7.9	2.06	10	4

TEM. Calcined catalyst samples (875 K for 24 h) were examined in a JEOL 2000 FX TEM at 200 keV. The TEM results we report are for those of the "oxidized" catalyst, not the reduced catalyst, so we are not seeing cobalt metal but cobalt oxide. The powders were dusted onto holey carbon film supported on copper grids. Elemental analysis was performed using a Tracor Northern energy dispersive spectroscopy system (EDS) equipped with a Be window X-ray detector. Quantitative analysis was performed using the standardless analysis program SMTF.

XPS. The XPS measurements were performed with a Leybold–Hereaus LHS-10 instrument equipped with a DS5 data acquisition system. This instrument has an auxiliary sampling port with an associated microreaction chamber (approx 30 cm^3) that allows samples to be treated at or above atmospheric pressure. This spectrometer uses a magnesium anode (Mg $K\alpha$ = 1253.6 eV) operated at 13 kV and 20 mA. The instrument operates at a vacuum of 2×10^{-9} mbar (2×10^{-7} Pa) or lower. The detection area on the sample was approximately 3 × 7 mm.

A thin 1-cm-diameter precalcined catalyst wafer, formed from the powdered catalysts after calcination at 875 for 24 h, was sandwiched between tantalum foils and attached to a Leybold–Hereaus heatable transfer rod. After insertion of the transfer rod into the reactor zone, a 5-min evacuation of the reactor was performed followed by the reduction treatment. The reduction was performed in a hydrogen flow with a flow rate of 10 cm^3/min. The temperature was programmed to ramp with a heating rate of 10 K/min to 673 K and held at 673 K for 16 h. The catalyst was then cooled in the hydrogen flow to room temperature. After completion of these treatments, the catalyst was transferred to the XPS analysis position via vacuum interlocks. This transfer was normally accomplished within 5 min. The reduced catalysts were also sputtered with Ar^+ for 10 min and reanalyzed. It was estimated that approximately 50 Å was removed from the surface based on sputtering

thin-film reference samples of similar composition under the same conditions.

The Co $2p_{3/2}$ transition was used to identify the cobalt species on the catalyst surface. For γ-alumina-supported catalysts, the Al $2p$ line from the alumina support was used as the binding energy reference (74.5 eV) for correction due to sample charging. For samples not containing Al_2O_3 the C $1s$ peak (284.6 eV) due to hydrocarbon contamination was used as a binding energy reference. The binding energies reported were found to be reproducible to ±0.2 eV. The Co $2p_{3/2}$ spectra were curve fitted using a damped nonlinear least-squares fitting program. The entire Co $2p$ region was not fitted because of the very poor signal/noise in the $2p_{1/2}$ region. This may lead to a small underreporting of the oxide contribution to the Co spectra, but this error is not believed to significantly alter the interpretation of the data. The curve-fitting results were used to calculate the particle-size-corrected extents of Co reduction and average Co particle sizes according to previously published methods (*13, 14*).

Catalyst Performance

TPD unit. Experiments of TPRx of CO, methanation, and TPSR were performed in the temperature-programmed desorption (TPD) unit. This apparatus is composed of a temperature programmer, mass flow controllers, a tubular reactor, a mass analyzer, and an IBM PC for data retrieval. The reactor temperature was programmed and controlled by a temperature programmer. The product gas is analyzed by the mass analyzer and recorded by the IBM PC. Details of this apparatus are described elsewhere (*15*).

TPRx. Before TPRx, the dried catalysts were reduced according to the following schedule: 100-mg samples were heated in 50 cm^3/min H_2 flow from room temperature to 423 K at a rate of 5 K/min, held there for 1 h, heated further to 473 K, held for an additional 1 h, and finally treated at 673 K in pure H_2 for 40 h. Following cooling to room temperature in a 30 cm^3/min helium stream, a number of CO (0.25 cm^3/pulse) pulses were injected to saturate the catalyst surface. The CO gas was preheated and kept at low pressure to prevent the formation of carbonyls. After the pulsing sequence, the system was flushed by a 30 cm^3/min helium stream for 10 min. The system was heated from room temperature to 873 K in a 30 cm^3/min hydrogen stream at a heating rate of 20 K/min. Peaks of m/e = 2, 15, 28, 30, and 44 were monitored during the heating process. The reactor was held at 873 K for 1 h (to remove the carbon residue from the catalyst surface), flushed with a 30 cm^3/min helium stream for 10 min, and cooled to room temperature. A second temperature program was performed, and no signals were detected.

Methanation. These experiments were performed over a temperature range between 503 and 543 K. A H_2/CO = 3/1 gas mixture was used as the reactant at a flow rate of 30 cm^3/min. The reduced catalyst was heated to 503 K and the temperature was then increased in steps. After each temperature step, the system was held for 10 min to reach a steady reaction rate. Peaks of m/e = 2, 15, 28, 30, and 44 were monitored continuously. Additional experiments were performed in which higher temperatures in the range studied were selected first to ensure that data collected at higher temperatures were not influenced by structural changes that may have occurred at lower reaction temperatures. The Arrhenius plots were reversible, an indication that no such structural modifications occurred. The maximum conversion did not exceed 7% for the most active catalyst. After the reaction sequence described above was performed, the system was flushed with a 30 cm^3/min helium stream for 5 min and cooled to room temperature. Blank runs over each support showed no activity over the temperature range 500–600 K.

The commercial cobalt tungstate was tested before reduction and after reduction. In the former case, 0.03 g of sample was

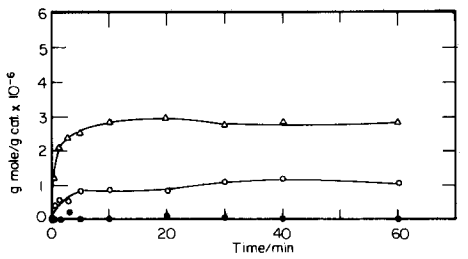

FIG. 2. Adsorption of Co^{2+} onto (△) Al_2O_3; (○) 12% WO_3/Al_2O_3; and (●) WO_3.

dehydrated in He (100 cm^3/min) while heating from 298 to 425 K at a rate of 5 K/min followed by a hold at 425 K for 1 h. The sample was reduced in H_2 (50 cm^3/min) at 675 K for 20 h following the dehydration procedures described above. Both samples were subjected to methanation studies using procedures identical to those used for the dispersed catalysts.

RESULTS

CATALYST PREPARATION

To test our hypothesis, catalysts of equivalent weight loadings had to be prepared on Al_2O_3, 12% WO_3/Al_2O_3, and WO_3 using similar procedures. Additional constraints were imposed. The pH of the impregnant needed to lie in the window of the pH of the pzcs of the pure supports in order to realize the pH-directed adsorption of the Co^{2+} precursor. Also, the weight loading of the finished catalysts should be in excess of ~5% to ensure sufficient reduction at modest temperatures (<775 K) so that enough metal is present to detect reaction product signals.

Preliminary experiments were conducted to establish the appropriate experimental conditions. Cobalt solutions with a concentration sufficient to mount 3% by weight of metal, assuming all the Co was transferred to the support, were prepared. Figure 2 shows the amount adsorbed as a function of time for these preliminary experiments. It is seen that adsorption equilibrium is attained in ~10 min. The amount adsorbed on Al_2O_3 is much greater than that on 12% WO_3/Al_2O_3; under these conditions virtually no adsorption occurs on WO_3. The weight loading on Al_2O_3 that corresponds to the plateau shown in Fig. 2 is ~0.02%, clearly demonstrating that the adsorption/exchange component of Co derived from wet impregnation is very small.

The rationale behind the pseudo-wet impregnation experiments was based on the assumption that the amount of Co adsorbed by exchange could be neglected compared to the amount deposited during the evaporation of electrolyte from within the pores. An excess of solution was used in the latter case to provide for a more homogeneous deposition of precursor that might better approximate the processes occurring during ion exchange (*15*). The metal content of each catalyst was determined by AA and results are presented in Table 2. The results show that similar weight loadings are obtained on all supports regardless of the method.

TPRd

Figures 3, 4, and 5 show the TPRd profiles for the dried cobalt catalysts with weight loadings of 1, 3, and 6% mounted on each support. Also shown is the TPRd spectrum for the unsupported precursor. For temperatures less than approximately 600 K, the following observations can be made.

Co/Al_2O_3: profiles with a peak temperature maximum that increases to higher tem-

TABLE 2

Cobalt Weight Loading on Supports Using Different Preparation Procedures

Catalyst	Procedure	Intended wt. loading %	Measured wt. loading %
Co/Al_2O_3	Dry	5.8	6.6
Co/Comp	Dry	5.5	5.3
Co/WO_3	Dry	5.7	6.2
Co/Al_2O_3	Wet	5.5	6.5
Co/Comp	Wet	5.6	6.2
Co/WO_3	Wet		4.8

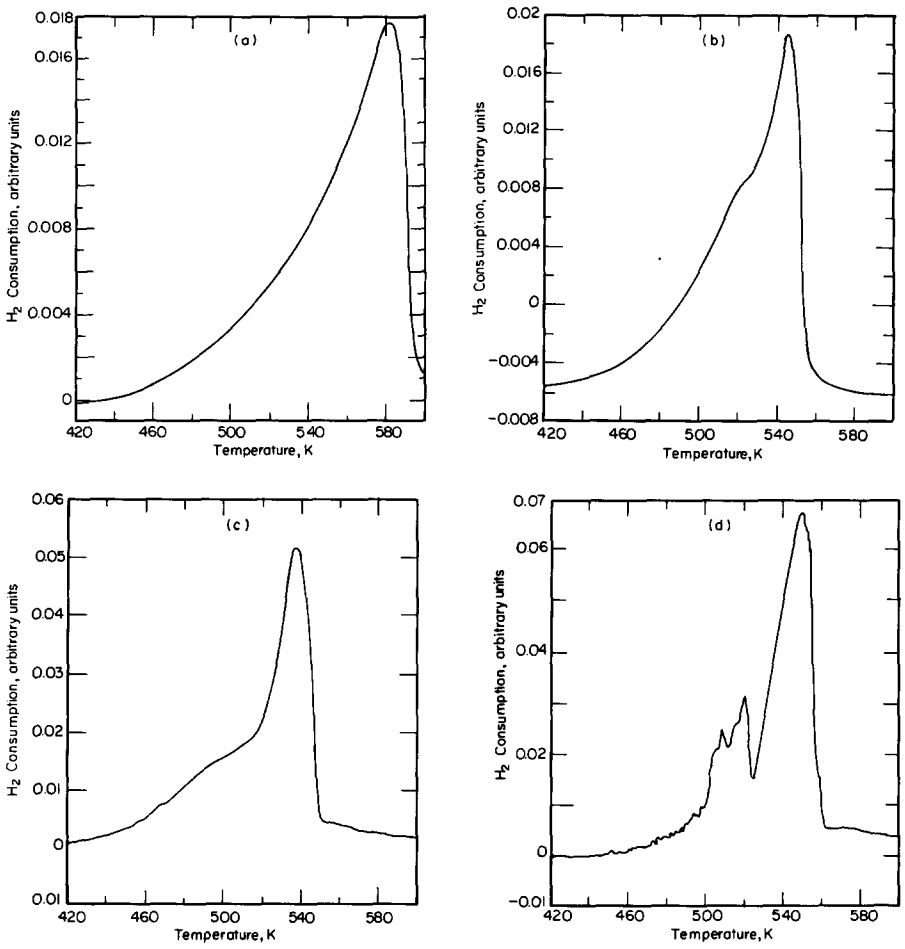

FIG. 3. TPRd profiles of dried precursors mounted on Al_2O_3: (a) 1% Co; (b) 3% Co; (c) 6% Co; (d) unsupported $Co(NO_3)_2$.

perature as the loadings *decrease* are observed.

Co/12% WO_3/Al_2O_3: profiles are seen in which the peak temperature maxima are not correlated with weight loading; the full-width at half maximum (FWHM) for each weight loading is greater than the FWHM for cobalt supported on each of the pure phases.

Co/WO_3: profiles with a peak temperature maximum that increases to higher temperatures as the loadings *increase* are observed. The analysis of TPRd profiles for multicomponent systems usually treats the problem of resolving interactions between two metals on a common support. In this case, TPRd profiles for the bimetal system are either the simple superposition of features seen for each metal on the same support *or* new features in the profile that might be attributed to, for example, a metal–metal interaction during reduction are seen.

The analysis of the data presented in Fig. 3–5 is complicated by several factors. First, the dispersed WO_3 does not have to have the same properties as its bulk counterpart; metal-support interactions revealed during TPRd might, therefore, have no "pure phase" analogue for comparison. Second, the "efficiency" of selective metal deposi-

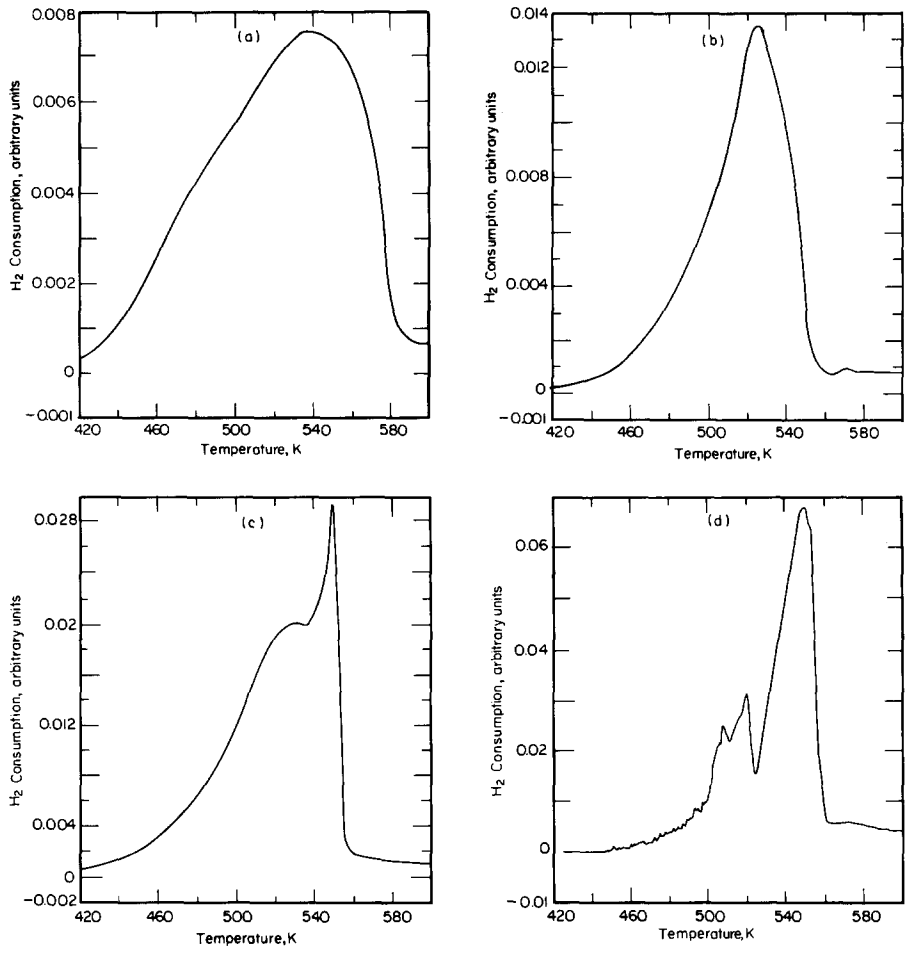

FIG. 4. TPRd profiles of dried precursors mounted on 12% WO_3/Al_2O_3: (a) 1% Co; (b) 3% Co; (c) 6% Co; (d) unsupported $Co(NO_3)_2$.

tion from the aqueous phase onto the WO_3 portion of the composite is unknown. Other factors, such as direct exchange with Al_2O_3 hydroxyl groups, could occur. Thus, the weight loading associated with each phase is unknown, and the results shown in Figs. 3 and 5 demonsrate that peak positions vary depending on loading and pure support. Finally, the results shown in Fig. 2 confirm that adsorption/impregnation of Co^{2+} on Al_2O_3 and the WO_3-modified carrier is not very favorable. Only 0.02% by weight is exchanged with Al_2O_3 and approximately one-third of this value is found on the 12% WO_3/Al_2O_3 composite. The TPRd experiments were performed on samples where weight loadings were orders of magnitude greater than those where adsorption results are available. We have no data on the adsorption properties onto these supports under pseudo-wet impregnation conditions. Collectively, such factors make it difficult to quantitatively evaluate the TPRd profiles of the composites. We have attempted to qualitatively interpret the composite profiles. The motivation was to provide reasonable confirmation that a fraction of the cobalt is associated with the second phase oxide (WO_3) despite the fact that only 12% by weight of the samples is WO_3 and the esti-

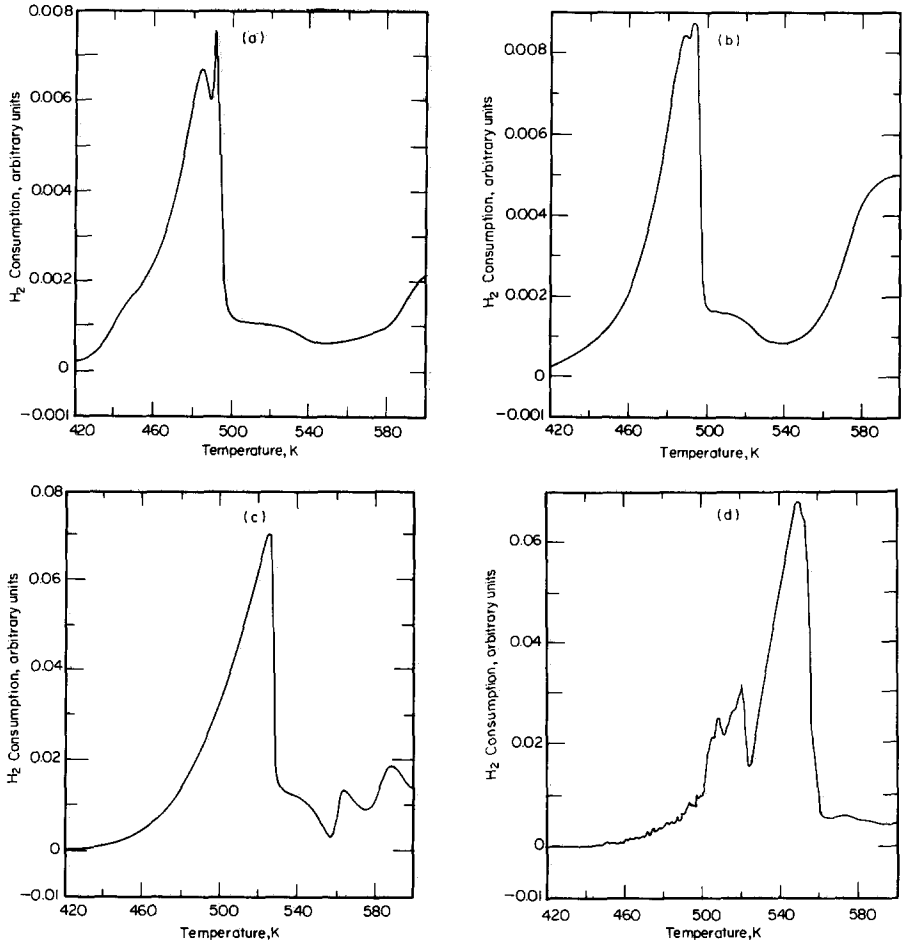

FIG. 5. TPRd profiles of dried precursors mounted on WO_3: (a) 1% Co; (b) 3% Co; (c) 6% Co; (d) unsupported $Co(NO_3)_2$.

mated surface area of WO_3 is only ~15 m^2/g (*8*).

The TPRd profiles for Co on the pure oxides were assumed to be Gaussian. The Levenberg–Marquardt method, which reduces the least-squares difference between the experimental profile of the composite and that of two Gaussian profiles, was employed (*16*). In this method, no assumption regarding the parameters of the Gaussian profiles (peak amplitude, position, and FWHM) are made. First, we examined the TPRd profiles from Al_2O_3 assuming that two Gaussian profiles could fit the data. Indeed, good fits could be obtained. However, the contribution from the "lower" temperature peak (most evident in Figs. 3b and 3c) was always less than 16% of the total area. Thus, we treated the Al_2O_3 contribution to the composite TPRd profiles (at each weight loading) as a simple Gaussian. The calculation was then reinitiated by selecting six parameters (3 for each Gaussian profile derived from the pure supports) and regression was then used to provide the best fit parameters. Figure 6, 7, and 8 show the experimental and calculated TRPd profiles for the composites with Co weight loadings of 1, 3, and 6%. Peaks were assigned to either the WO_3 or Al_2O_3 mounted Co based on the "close-

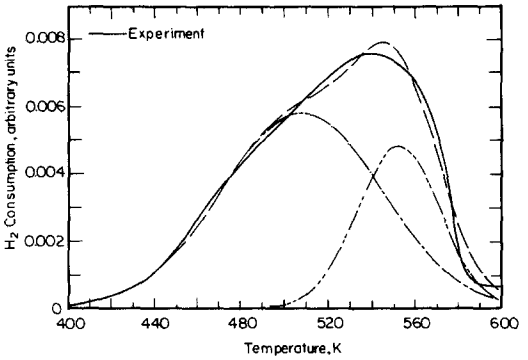

FIG. 6. Experimental TPRd profile of 1% Co on 12% WO_3/Al_2O_3 and "best fit" assuming a two-Gaussian decomposition. Assignment: (–·–) WO_3; (----) Al_2O_3.

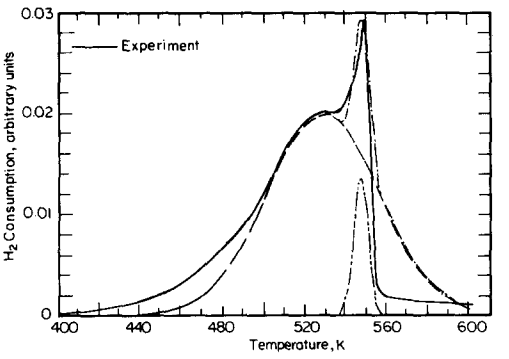

FIG. 8. Experimental TPRd profile of 6% Co on 12% WO_3/Al_2O_3 and "best fit" assuming a two-Gaussian decomposition. Assignment: (–·–) WO_3; (----) Al_2O_3.

ness" of the peak temperature maximum of the computed and experimental curves, and the properties of these curves were examined. Table 3 gives the fraction of Co at each weight loading that is associated with WO_3. Also presented are the temperatures of the peak maxima for the computer-derived curves and the corresponding experimental temperatures for the profiles from the pure phases. The uncertainty of all the parameters was less than 10%. When we tried to improve these results by using three Gaussian peaks, the quality of fits was poor.

The general findings are that a substantial fraction of the Co strongly interacts and resides on the second phase WO_3. This occurs despite the fact that only 12% by weight of the samples is WO_3 and the estimated surface area of WO_3 is only ~15 m^2/g (*8*). The variation in peak temperature maxima from sample to sample are in reasonable agreement with those from the pure supports but they show no discernible trend, which might be a reflection of the fact that the properties of WO_3 *and* Al_2O_3 in the composite are different from their bulk-phase counterparts.

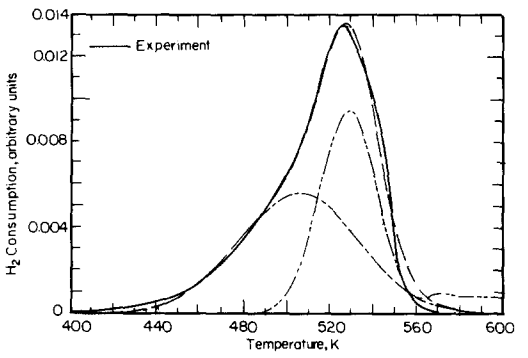

FIG. 7. Experimental TPRd profile of 3% Co on 12% WO_3/Al_2O_3 and "best fit" assuming a two-Gaussian decomposition. Assignment: (---) WO_3; (----) Al_2O_3.

TEM

12% WO_3/Al_2O_3. The TEM results of a WO_3/Al_2O_3 composite with a 12 wt% loading of WO_3 showed that 0.5- to 0.8-nm particles are present on the composite surface. The particle size was not affected by electron beam exposure after the minimum exposure that is usually necessary to focus and perform the astigmatism correction before recording the image. However, we cannot rule out the possibility that these clusters are the result of electron beam aggregation of the dispersed phase.

6% Co/WO_3. The sample showed particles of a Co-containing phase that generally exists independent of WO_3. In fact, some regions showed single crystals of a Co-containing phase ranging in size from 30 to 40 nm. Diffraction experiments conclusively identified Co_3O_4 as the cobalt phase.

TABLE 3

Results of Peak Fitting

Catalyst	Support assignment	Peak Temperature K		Estimated % of Cobalt on WO_3
		Fit	Experiment	
1% $Co/WO_3/Al_2O_3$	WO_3	505	492	71
	Al_2O_3	552	583	
3% $Co/WO_3/Al_2O_3$	WO_3	507	495	55
	Al_2O_3	528	547	
6% $Co/WO_3/Al_2O_3$	WO_3	529	526	92
	Al_2O_3	547	537	

6% Co/Al_2O_3. Figure 9 shows that, on Al_2O_3, Co particles are poorly dispersed with particle size in the range of 16–30 nm (average 19 nm). The Co particle size is very nonuniform; diffraction experiments confirmed that cobalt exists as Co_3O_4. EDS spectra were measured from small, thin particles of support where the absence of Co_3O_4 particles could be checked visually. Of six areas examined, two showed no Co peak at all and the others ranged from 0.84 to 1.19%. When Co_3O_4 particles were obviously present, the analysis indicated 4 and 4.6% Co. These numbers are not precise because a standardless analysis was used, but the trend indicates that even when Co particles are not seen, some Co is present.

6% Co/12% WO_3/Al_2O_3. On the composite the particle sizes range from 60 to 80 nm (average 76 nm) indicating a poorer dispersion, but the relative standard deviation indicates that the Co crystallite size distribution is approximately twice as uniform when compared to Al_2O_3 (see Fig. 10). This could be interpreted on the following basis. Some of the $Co(NO_3)_2$ may interact with the WO_3 to form a Co^{2+}–WO_3 species, while the remaining $Co(NO_3)_2$ agglomerates to form large particles. It is possible that the pzc of the WO_3-modified carrier (more acidic) is responsible for the formation of large $Co(NO_3)_2$ particles, which become large Co_3O_4 crystallites following calcination. The uniformity of the particle size distribution may simply be due to the fact that extremely large Co_3O_4 particles are formed. On the composite sample, areas that had obvious particles of Co_3O_4 showed Co at a level of ~4%. The thin areas had analyses as follows: 0.9, 1.2, 0.5, 1.2, 1.8, and 0.9, suggesting again that there is dispersed Co in addition to the large particles. These areas also showed W to be present. This strongly suggests that the dispersed second-phase oxide (WO_3) serves as nucleation centers for a better dispersed Co phase.

XPS

Co_3O_4. The cobalt oxide standard showed the Co $2p_{3/2}$ peak indicative of the oxide at 780.5 eV. After reduction, this downshifts to 778.2 eV indicative of metallic cobalt.

$CoWO_4$. We find that Co is totally reduced to metallic Co and tungsten is partially reduced to metallic W. The spectra are much less complicated than the oxide-supported spectra in that we do not observe the differential charging that produced two sets of peaks for each of the reduced species as described below.

Co/WO_3. Comparing the XPS spectra of the catalyst with that of Co_3O_4 indicates that the Co is in the form of Co_3O_4. It is totally reducible to metal. There is an increase in the Co 2*p*/W 4*f* intensity ratio when the catalyst is reduced.

Co/Al_2O_3 (Fig. 11). The calcined catalyst

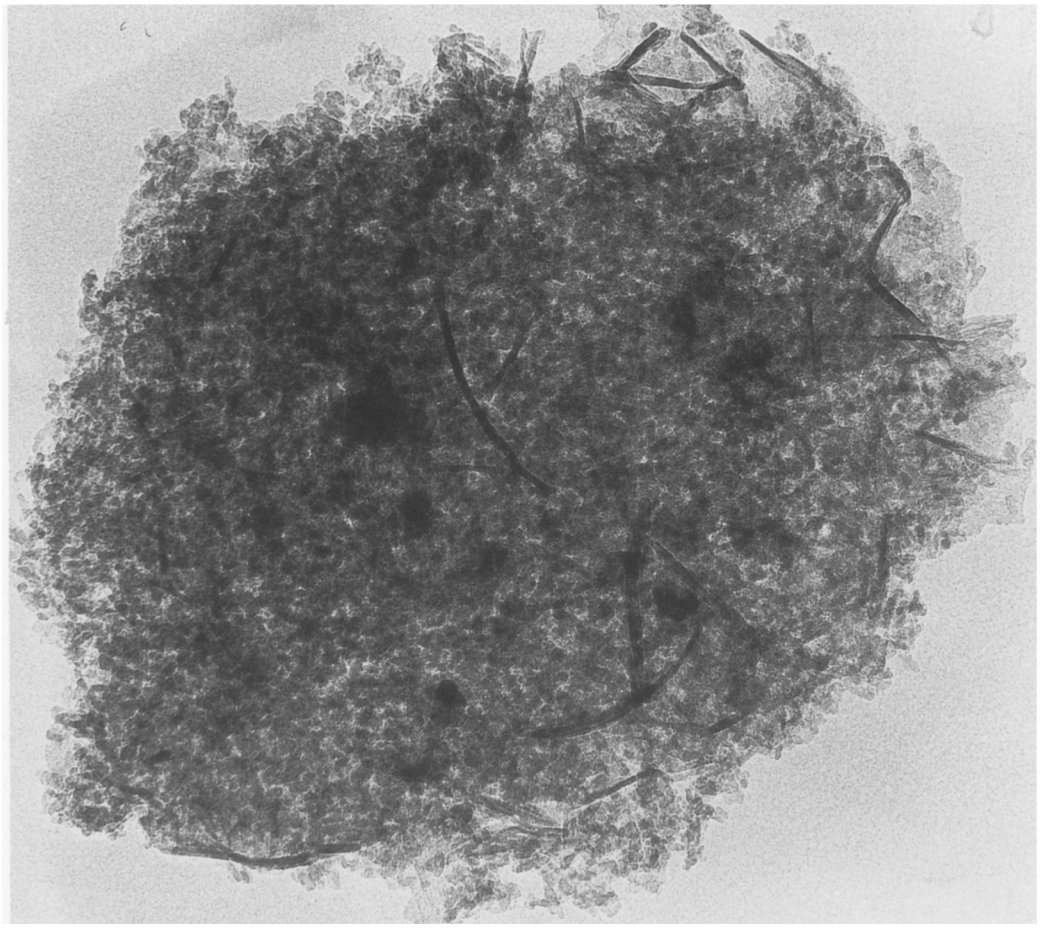

FIG. 9. TEM micrograph of 6% Co/Al_2O_3 catalyst. Note nonuniformity of cobalt particle size.

contains primarily Co_3O_4. When the catalyst is reduced, Co_3O_4 is converted to Co metal; however, there remains a nonreducible Co_{ox} with higher binding energy and a prominent shake-up satellite peak, likely due to $CoAl_2O_4$ (*17*). The difference in binding energy for metallic Co in the supported catalysts compared to reduced Co_3O_4 or Co/WO_3 may be due to differential charging between Co^0 and the Al_2O_3 support, which was used as a reference (Al $2p$ = 74.5 eV). An unusual phenomenon is observed in the Co $2p$ spectra of the reduced catalyst shown in Fig. 11 that has sometimes been observed previously in our laboratory during the reduction of Co/Al_2O_3 catalysts. A peak appears at approximately 3.4 eV lower than the 777.4-eV peak assigned to Co^0. This is due to Co^0 that is in electrical contact with the sample holder and does not charge. When the catalyst is sputtered, some of the electrical contact is broken, and the major metallic Co peak is at 777.7 eV. The Co^0/Al $2p$ intensity ratio is observed to increase on sputtering, in contrast to an observed decrease in the Co_{ox}/Al $2p$ intensity ratio.

$Co/12\%$ WO_3/Al_2O_3 (Fig. 12) The composite-supported Co catalyst is unlike that of either its Al_2O_3 or its WO_3 counterparts. An observed higher binding energy for Co and the presence of a prominent shake-up peak characteristic of Co^{2+} indicates that

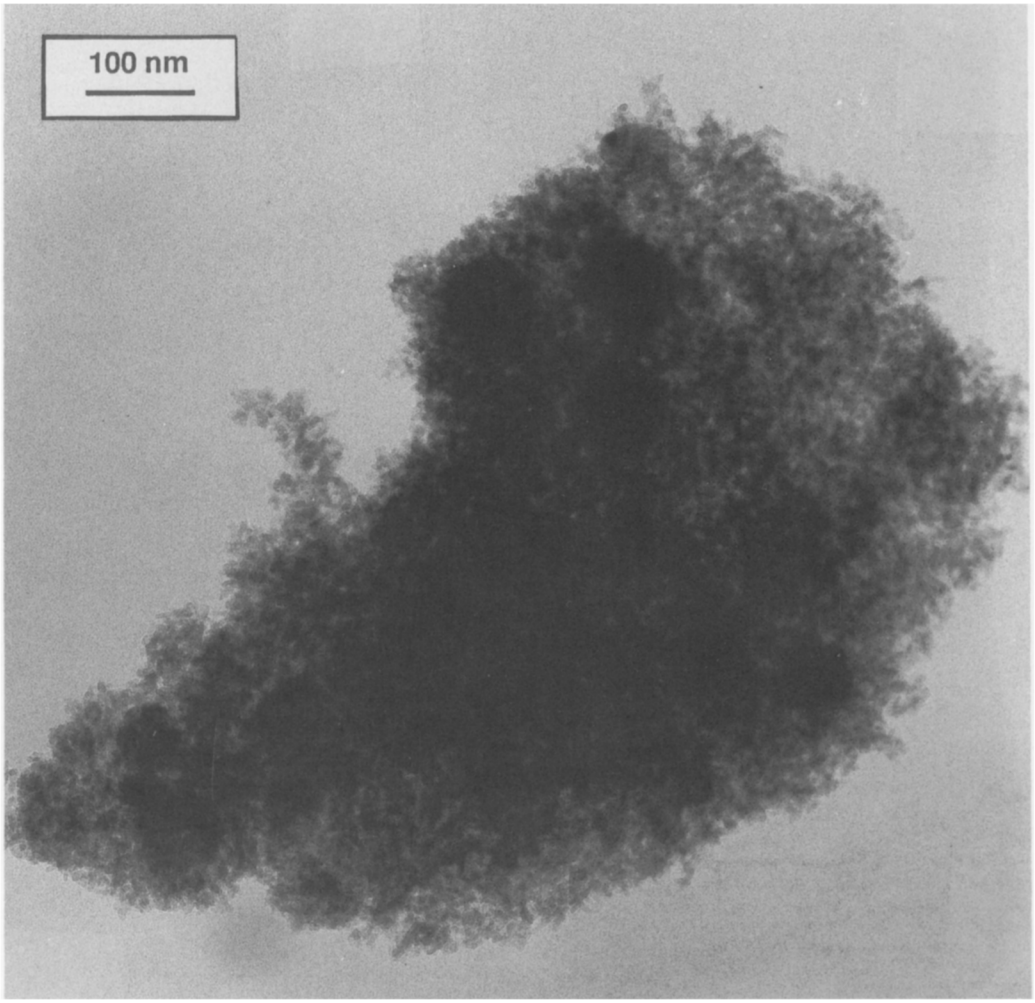

FIG. 10. TEM micrograph of 6% Co on 12% WO_3/Al_2O_3.

a relatively larger area is occupied by this species on the surface of the composite catalyst than that of Co/Al_2O_3. The reducibility of Co in this catalyst is the lowest, but calculations show the metallic Co crystallite size to be only slightly greater in the composite catalyst compared to Co/Al_2O_3 following reduction.

Tungsten is nonreducible in all of the catalysts. The spectra do change significantly because of both increases in W intensity in some cases and also a decrease in surface charging on reduction and a further decrease in charging after sputtering. This is evidenced by increased resolution of the W 4*f* doublet and a simultaneous decrease in FWHM of the Al 2*p* peak for the composite-supported catalyst (*2*).

A summary of the Co $2p_{3/2}$ binding energies for the cobalt oxide and metallic phases and average Co^0 crystallite sizes calculated from the XPS results are presented in Tables 4A, 4B, and Table 5.

Additional insight into the disposition of Co in these catalysts subsequent to the treatment procedures can be obtained by a quali-

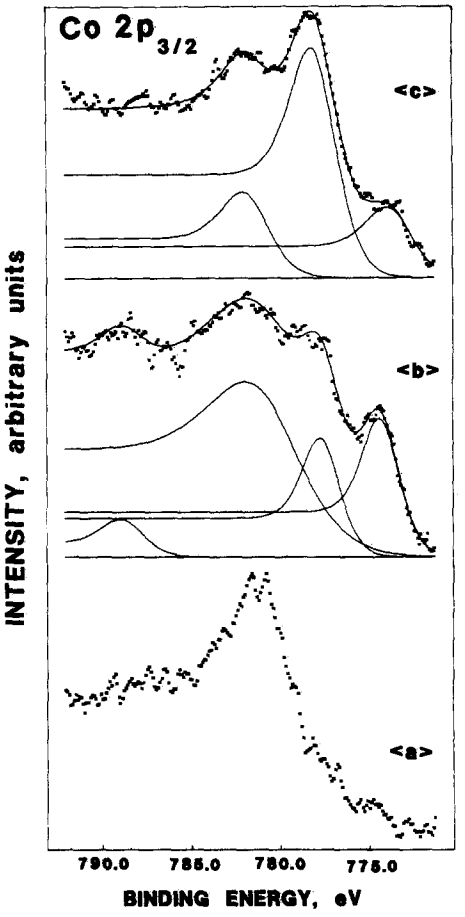

FIG. 11. XPS spectra of Co/Al_2O_3 following treatment conditions described in text.

tative examination of intensity ratios. These results, which are the averaged values from three analyses, are compiled in Table 5. The cobalt/aluminum ratio decreases for both the Al_2O_3 and composite-supported Co catalysts after reduction.

CATALYST PERFORMANCE

The CO TPRx spectra for each catalyst are shown in Fig. 13. By 600 K, virtually all the adsorbed CO is removed as CH_4 (small amounts of CO_2 were detected) over the Al_2O_3 and composite oxide-supported Co catalysts. However, for Co/WO_3, there always appeared a high-temperature tailing despite the fact that a discernible and reproducible peak appears at ~435 K. Since these spectra are used to estimate the number of active sites, some explanation for the behavior seen in Fig. 13c was sought. We show elsewhere that TPRd profiles for bulk WO_3 and weight loadings from 30 to 2% WO_3/Al_2O_3 show a progressively higher onset of reduction temperature (*18*). The catalysts used in this study were reduced in pure H_2 at 673 for 40 h, while the TPRd results are obtained for 8½% H_2/Ar. The actual onset of reduction in the case that pure H_2 is used is not known; however, it is likely that the order of reducibility should proceed: WO_3 (bulk) easier than WO_3 (supported). Such a conclusion is consistent with results reported by Kadkhodayan and Brenner (*19*).

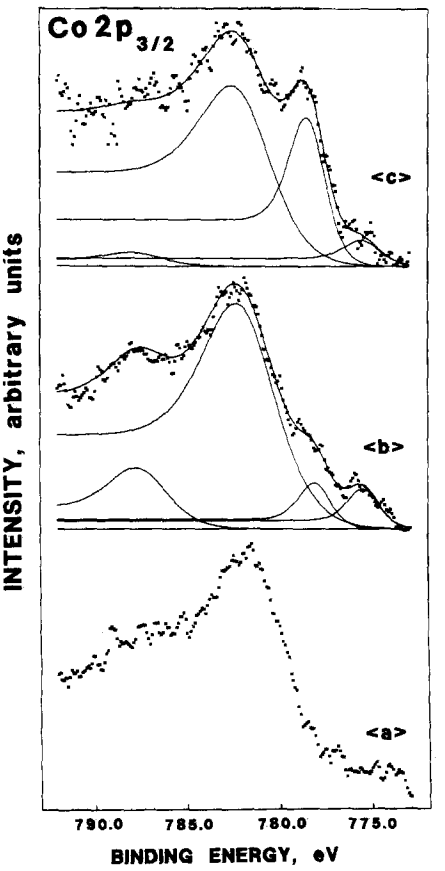

FIG. 12. XPS spectra of $Co/12\% WO_3/Al_2O_3$ following treatment conditions described in text.

TABLE 4

Binding Energy of Co $2p_{3/2}$

	A. Higher binding energy peak due to Co Oxide (eV) Before reduction	After reduction	After sputtering
Co_3O_4	780.5	[a]	
Co/Al_2O_3	781.1	780.7	781.5
$Co/WO_3/Al_2O_3$	781.7	781.7	781.6
Co/WO_3	780.5	[a]	
	B. Lower binding energy peak due to Co^0 (eV) After reduction		After sputtering
Co_3O_4	778.4		778.3
Co/Al_2O_3	777.4		777.7
$Co/WO_3Al_2O_3$	777.6		777.7
Co/WO_3	778.2		778.2

[a] No Co oxide remained after reduction.

In a separate set of experiments, a WO_3 support was subjected to a TPRx experiment following our standard procedures. The results showed that CH_4 was evolved at temperatures higher than ~550 K. Thus, we attribute the area labeled II in Fig. 13c to CO hydrogenation on a reduced portion of WO_3. It is important to note that any contribution to CH_4 formation from WO_3 alone under the steady-state conditions of our experiments will be negligible because the highest reaction temperature was less than 550 K and bulk WO_3 has a very low activity at this temperature and dispersed

TABLE 5
XPS Data for Treated Co Catalysts

Sample	Treat condition	$I_{Co\,2p_{3/2}}/I_{Al\,2p}$	$I_{Co\,2p_{3/2}}/I_{W\,4f}$	$I_{W\,4f}/I_{Al\,2p}$	Co^0 size (nm)
Co/Al_2O_3	a	0.32			
	b	0.12, metal 0.17, oxide			14.6
	c	0.24, metal 0.07, oxide			7.7
$Co/WO_3/Al_2O_3$	a	0.58		0.70	
	b	0.07, metal 0.41, oxide		1.23	20.3
	c	0.16, metal 0.28, oxide		1.59	9.7
Co/WO_3	a		1.85		
	b		3.67		
	c		3.04		

Note. Intensity ratios were measured with a precision of ±10% (rsd) or better. Treatment conditions: (a) Sample was calcined at 875 K for 24 h in the furnace; (b) calcined samples were reduced at 675 K for 16 h in H_2; (c) reduced samples were sputtered with argon ions for 10 min.

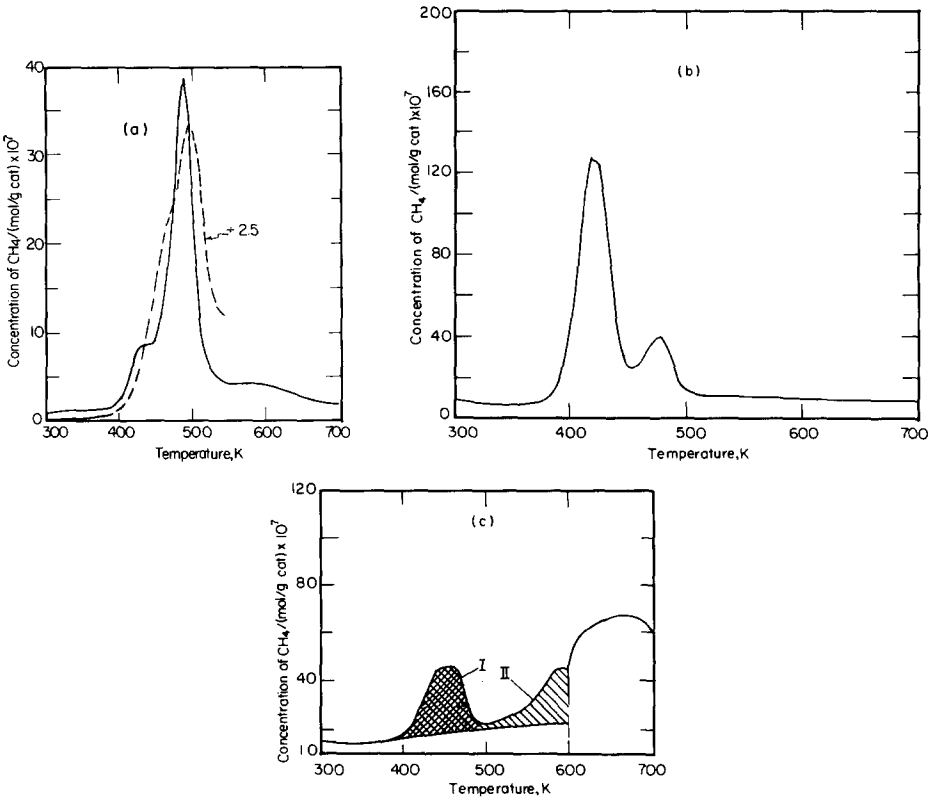

FIG. 13. CO TPRx spectra for 6% cobalt catalysts on (a) Al_2O_3; (b) 12% WO_3/Al_2O_3; (c) WO_3. See text for discussion of superimposed TPSR spectra in (a) regions labeled I and II in (c).

WO_3 is not reduced at this temperature. The apparent absence of any reduced tungsten in our XPS results is probably due to the shorter treatment time (cf. 40 h vs 16 h) in hydrogen.

The bulk $CoWO_4$ sample showed a very interesting activity pattern. In its dehydrated (nonreduced) state, it exhibited a high reactivity, comparable to that of Co/WO_3. For example, at 535 K the activity for the $CoWO_4$ (nonreduced) and Co/WO_3 (reduced) were 460 and 470 μmol CH_4/g · min, respectively.[3] The activity at each temperature reached a steady value, showing little to no deactivation; its reactivity was reversible when the temperature was either increased or decreased. On the other hand, a stable reactivity measurement for the reduced $CoWO_4$ sample could not be obtained. At the lowest reaction temperature (~500 K) its activity was high but showed a sharp decrease with increasing time on stream (~10 min). When the temperature was raised, the same behavior was observed. These results suggest that: (1) on the surface of this commercial sample, there are Co–W species that are active in methanation, (2) the nonreduced sample is not reduced under reaction conditions or otherwise its behavior would have been similar to the reduced sample. We return to this point shortly.

A qualitative scenario emerges. The composite oxide has the lowest temperature TPRx peak maximum and no adsorbed CO remains on the composite catalyst at tem-

[3] The densities of these materials are approximately the same, which provides resonable justification for comparing activities on a weight basis.

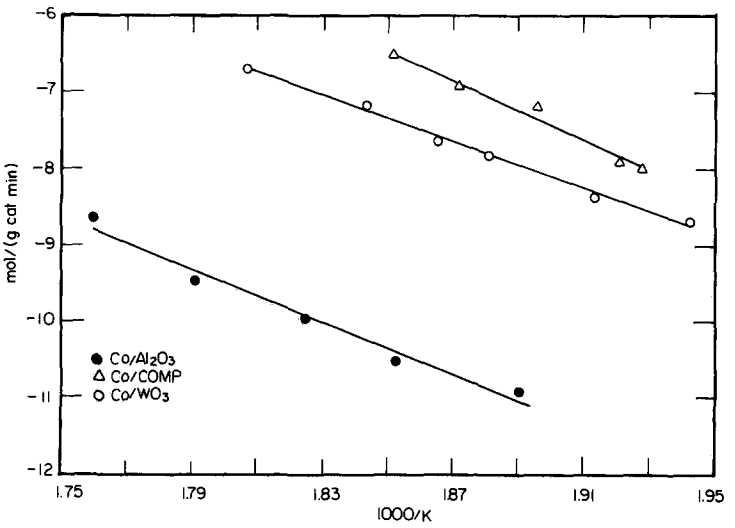

FIG. 14. Arrhenius plots of methanation rates for 6% Co catalysts on WO_3, Al_2O_3, and 12% WO_3/Al_2O_3.

peratures greater than 500 K, the lowest temperature used for steady-state reaction studies. This peak maximum temperature is followed by the WO_3 and then the Al_2O_3-supported cobalt. Based on previous observations (*20*), we would expect that the methanation activity per gram of catalyst would be highest over the composite followed by the WO_3 and then the Al_2O_3-supported cobalt. Indeed, this is what is found. Figure 14 shows Arrhenius plots of the methanation rate based on 1 g of catalyst. We present the data in this form because we still need to establish a basis for evaluating the number of active sites, which we do shortly. The solid lines are least-squares fits to the data.

TABLE 6

Activation Energy and Total Active Sites for CO Hydrogenation

Catalyst	A. Activation energy of CH_4 formation (Kcal/mol)	B. Total active sites
Co/Al_2O_3	34.6	1.9×10^{18}
$Co/WO_3/Al_2O_3$	38.4	5.5×10^{18}
Co/WO_3	25.7	9.8×10^{18}

We see that the activity decreases in the order composite $>WO_3>Al_2O_3$. Table 6A summarizes the values of the activation energies determined from the data in Fig. 14. Table 6B provides our estimates of the number of active sites on each catalyst based on CO–TPRx results; 1 : 1 stoichiometry was assumed. Table 7 reports TONs evaluated at 540 K for each catalyst. The activity decreases in the order composite $>WO_3>Al_2O_3$. The intrinsic activity of Co is the same for those catalysts that contain WO_3, whether WO_3 is present in the form of dispersed clusters anchored on Al_2O_3 or on bulk particles acting as the catalyst carrier. We had difficulty estimating the number of active sites on $CoWO_4$; therefore, no TON is reported for this sample. All catalysts produced some ethane with an activity varia-

TABLE 7

Activity of Supported Co Catalysts

	Temperature (K)	TON
Co/Al_2O_3	540	0.014
$Co/WO_3/Al_2O_3$	540	0.27
Co/WO_3	536	0.26

tion, per gram of catalyst, in the same order as their methane formation rate; however, the values were approximately two orders of magnitude smaller than the methane values.

The TPSR spectra subsequent to steady-state methanation reveals the carbon inventory that develops on the catalyst surface during reaction. A part of this inventory could be either undissociated CO or various forms of CH_x (x = 0–3). The former would be removed from the surface as CH_4 appearing over a temperature range corresponding to that of a CO–TPRx experiment; the latter would be evolved as CH_4 in temperature ranges corresponding to the reactivity of the CH_x residue. We find that above 600 K, methane is removed from the surface of each catalyst in a complex fashion as indicated by many peaks in the spectra. The CH_x pool is assumed to be the source of this CH_4. The maximum amount comes from the composite catalyst. Below 550 K, the maximum reaction temperature, there is virtually no methane released from the composite and the WO_3-supported catalysts. This suggests that all carbon-containing species are rapidly removed under reaction conditions, prior to TPSR. However, the Al_2O_3-supported catalyst releases methane in a peak whose shape and position are identical to that found for its CO–TPRx experiment. This is shown in Fig. 13a. The area under this peak in the TPSR spectrum is approximately twice the area under the CO–TPRx spectrum. The higher capacity for carbon retention in the form of CO for this catalyst could be due to the fact that more CO is adsorbed when exposed to the catalyst surface in the presence of H_2 under reaction conditions when compared to He under TPRx conditions (*21*). Collectively, these results demonstrate that CO dissociation on cobalt for the composite and for WO_3 supports is much easier than that for Co supported on Al_2O_3. The differences in CO activation seen in these catalysts are likely due to the chemical/structural nature of the active site(s).

DISCUSSION

At the outset, we reiterate the two objectives of this study. We sought to demonstrate that a pH-directed selective metal-support exchange could be realized when catalyst preparation conditions were carefully considered. A number of recent studies have attempted to establish the mechanism(s) for CO adsorption and hydrogenation that operates on alumina-supported catalytic metals (*22*). These studies employed various sequences of reactant adsorption followed by different schedules of temperature-programmed desorption while monitoring the release of methane. Lee and Bartholomew (*21*) have provided a scenario for the reactive pathways similar to that proposed by Falconer and co-workers (*22*): (1) CO dissociation on the metal followed by hydrogenation of carbon; (2) spillover of CO and H to the support where a CH_xO complex is formed followed by diffusion of the complex to metal crystallites where it decomposes. *Both reactions take place on metal sites.*

Our experiments were conducted on cobalt catalysts using a single heating rate and a single set of TPRx conditions. Our second objective is to establish the properties of a catalytic metal, such as cobalt, when it is dispersed on a second-phase oxide, not to establish mechanistic pathways. However, our results are completely consistent with previous results. We find two methane peaks in the TPRx spectra from the alumina and composite oxide supported catalysts. The origin of the peaks has been the basis for interpreting mechanistic pathways. Examination of Fig. 13 shows that there are significant downshifts in the peak temperature maxima for the two CH_4 peaks from the composite compared to the alumina-supported catalyst. This finding implies that the rate-limiting steps of all reactive pathways are altered, and this we attribute to the active centers that result when cobalt is supported on the second-phase oxide.

The hydrogenation of carbon monoxide on cobalt catalysts has been known to be

affected by two factors: the cobalt loading (or particle size) (*23, 24*) and the extent of reduction (*25, 26*). These two factors are dependent on each other in that the extent of reduction is determined by, among other things, the cobalt weight loading. Recently, Lee *et al.* (*27*) reported that from their TEM results the particle sizes varied only slightly with reduction conditions and that the average particle size was about 20 nm at a constant cobalt loading of ~10% by weight.

The structure-sensitive nature of CO hydrogenation on supported cobalt catalysts has been interpreted by the following reasoning. As dispersion increases, the relative concentrations of the surface sites with lower coordination (e.g., planar sites) decreases and this results in a catalyst whose CO dissociation properties are poor. Kellner and Bell (*28*) and Mieth and Schwarz (*20*) attributed the higher activity of more poorly dispersed catalysts to electronic effects related to enhancement in the π backbonding contribution into the CO antibonding $2\pi^*$ orbital resulting in a weakening of the C–O bond.

Based on the above observations, we must first examine whether particle size differences can be the source of the enhanced activity of cobalt supported on the composite oxide compared to cobalt supported on Al_2O_3. A detailed study of particle size effects on the composite support is not available; thus our conclusions must be inferred from Co/Al_2O_3 results where data are available. Our TEM results show that the average particle sizes for the calcined catalysts are 17.8 nm for Co/Al_2O_3 and 77 nm for $Co/12\%\ WO_3/Al_2O_3$. Experimentally, we are unable to perform *in situ* reduction in the TEM, so particle sizes in the reduced state of the catalyst must be estimated. This estimate was performed at two levels for the Co/Al_2O_3 catalyst. Reuel and Bartholomew (*23*) report the extent of reduction as a function of Co weight loading. We interpolate their data to the 6% weight loading of our catalyst and use the CO–TPRx data to estimate the particle size on the reduced Co/Al_2O_3 catalyst. The value we calculate is 22 nm in excellent agreement with the conclusions reached by Lee *et al.* (*27*) cited earlier. We must be careful in using TPRx data for such estimates because the controversy relates to the origin of the two peaks in the spectrum. Using the XPS data and previously published methods (*13, 14*), we arrive at a particle size of 14.6 nm, which is also in reasonable agreement with the value determined above.

We still do not know the particle size of Co on the composite oxide. However, based on the reasonable agreement observed for Co/Al_2O_3, the Co^0 particle size may be estimated using the XPS results (*13, 14*) and the CO–TPRx data. The former calculation yields a particle size for the reduced catalyst of 20 nm and for the latter a value of 22.4 nm.

The estimated values of particle sizes for Co^0 on Al_2O_3 and the composite appear to be internally consistent whether XPS data alone or XPS/TPRx data are used as a basis for the calculations. Due to the similarity in computed/estimated particle sizes, structural sensitivity in its usual context appears to be inconsistent with explaining the 20-fold enhancement in TON seen for the composite oxide-supported cobalt catalyst compared to Co/Al_2O_3. This higher intrinsic activity seen for the tungsten-containing catalysts must be related to their ability to activate CO bond breaking, which would be followed by a rapid reaction of surface hydrogen with nascent carbon. While this "fact" appears to be evident, a more detailed understanding is not directly apparent from the data available. However, we can speculate as to the origin of the enhancement in activity seen, and this we do below.

The introduction of W onto the Al_2O_3 support results in a redistribution of Co phases compared to Co/Al_2O_3. Initially, the higher Co $2p_{3/2}$ intensity ratio for the unreduced composite catalyst compared to Co/Al_2O_3 might lead one to conclude that Co is better dispersed on the composite catalyst. However, upon closer examination of the trends

in Co/Al intensity ratios for the metal and oxidic phases of the reduced catalyst systems in Table 5, one can observe distinctly different trends in Co particle size for these phases caused by the prior deposition of W.

The formation of an unreducible oxide phase in the composite catalyst appears to be greater than that of Co/Al_2O_3. Indeed, the proportion of Co^{2+} observed in the XPS spectra of the as-prepared catalyst (indicated by a more pronounced satellite peak to the higher binding energy site of the main Co $2p_{3/2}$ peak) is greater than that of Co/Al_2O_3, accompanying the observed decrease in reducibility of the composite catalyst compared to Co/Al_2O_3. Combined, these observations may initially lead one to conclude that there is a greater proportion of the nonreducible $CoAl_2O_4$-like species formed on the surface of the composite catalyst. However, the activity data are not consistent with an increase in formation of a Co^{2+}–W interaction species. A Co^{2+}–W interaction species, like $CoAl_2O_4$, would be well dispersed and contribute to the higher Co_{oxide}/Al intensity ratio for the reduced composite catalyst compared to Co/Al_2O_3.

To examine the possibility that some type of Co–W interaction species may have been formed, activity measurements were conducted on $CoWO_4$, and it was found that the unreduced sample had an activity that was comparable to Co/WO_3. XPS reduction studies of $CoWO_4$ were also conducted under the same conditions used for reducing the composite catalyst. First, prior to reduction, the characteristic satellite due to Co^{2+} was very pronounced in the Co $2p_{3/2}$ spectrum and the binding energy of the Co (781.9) was nearly identical to that observed for the composite catalyst. However, it was also discovered that Co in $CoWO_4$ was totally reducible to metallic Co, and W was partially reducible to metallic W.

Formation of $CoWO_4$ in the composite catalyst would then contradict the decrease in reducibility of Co observed for this catalyst. Nevertheless, this apparent contradiction may not preclude the formation of a Co–W interaction species on the Al_2O_3 support. Salvati *et al.* (*2*) observed that when tungsten is distributed at less than monolayer coverage on Al_2O_3, it is nonreducible. On the composite catalyst at less than a monolayer coverage of W, it is unreducible, and this may in turn hinder reduction of Co that is in contact with the tungsten phase. At the same time, Co in interaction with W would yield XPS spectra more compatible with $CoWO_4$ than Co_3O_4 prior to reduction. Although the Co–W interaction species may be inert toward reduction, it may exhibit higher activity, as observed for $CoWO_4$.

The metallic Co particle size, based on XPS results alone, appears greater in the reduced composite catalyst than in reduced Co/Al_2O_3. Although the Co/Al intensity ratio would be expected to be less in the composite catalyst due to less formation of reduced Co, the decrease in intensity ratio compared to reduced Co/Al_2O_3 cannot be explained by this phenomenon alone. A greater particle size for Co in the composite catalyst is consistent with a larger Co_3O_4 particle size observed in the composite catalyst than in Co/Al_2O_3 by TEM for the oxide catalyst. When either the reduced composite catalyst or the reduced Co/Al_2O_3 are sputtered, the oxide component decreases as expected since it is initially well dispersed and more amenable to sputter removal. In contrast, the Co component on the surface of each catalyst increases on sputtering and decreases in average particle size. Such behavior may be due to exposure of more finely divided metallic Co beneath the surface of the catalyst and destruction by the sputtering process of the large metallic Co particles initially formed on reduction. We rule out the possibility that the 76-nm particles on the oxidized composite catalysts spread out over the WO_3 surface to form smaller particles after the reduction.

A brief explanation for the apparent decrease in Co particle size upon reduction of the composite catalyst is in order. Since XPS calculations result in an average particle size estimate, XPS cannot determine the

fraction of Co metal present as large particles versus small. One possible explanation for the difference in Co metal particle size expected from TEM results for the oxidic composite catalyst and XPS data for the reduced composite catalyst involves the reducibility of the Co^{2+}–W phase. Results for the $CoWO_4$ sample showed that Co is completely reduced to Co metal. While it is not known whether the supported Co^{2+}–W phase is reducible, the discrepancy in particle size for the oxidic (76 nm) and reduced (20 nm) cobalt particles suggests that the average Co metal particle size is due to a reduction of large (76 nm) Co_3O_4 crystallites and part of the highly dispersed Co^{2+}–W surface phase. Thus, the reduced composite catalyst may contain large Co metal crystallites from reduction of the 76-nm Co_3O_4 particles, small Co metal particles from a reduction of a fraction of the Co^{2+}–W surface phase, unreduced Co^{2+}–W surface phase, and unreduced $CoAl_2O_4$-like species.

It is tempting to attribute the higher activity of the composite to the presence of $CoAl_2O_4$-like species, which could promote CO dissociation in the same manner that $NiAl_2O_4$-like species were found to do in earlier studies (*15*). However, the intrinsic activity of Co/WO_3 was identical to the Co/ composite catalyst and the activity of unreduced $CoWO_4$ was comparable to that of Co/WO_3, which makes any explanation based on $CoAl_2O_4$-like species causing enhanced activity unlikely. Finally, we are left with the possibility of formation of a Co^{2+}–W species, the presence of which would be consistent with our arguments presented above. To examine this possibility further, we first discuss effects that occur during the initial preparation of the catalysts.

The equilibrium adsorption results on each support (Fig. 2) show that only a small amount of Co^{2+} ions is transferred to the solid phase. In the case of Al_2O_3 this is expected; the experiment was conducted at a pH ~6, which is below its point of zero charge. The net charge on the surface is positive, and the existence of any adsorption suggests that direct exchange with surface hydroxyls is the mechanism for adsorption. Such a process is generally unfavorable. On the other hand, we see virtually no adsorption on WO_3. This experiment was conducted at a pH ~6, which is above the pzc of WO_3 (≈4 (*8*)) so that the net charge on its surface is negative. However, the very low surface area of WO_3 (~1 m^2/g (*8*)) results in negligible adsorption of Co^{2+} on WO_3. The composite oxide shows what appears to be an intermediate behavior as far as its adsorption uptake is concerned. This result could be due to several factors. The pzc of this composite is ~6 (*8*), which would suggest that Co^{2+} ions in the bulk solution at pH ~6 would experience only a small, if any, driving force for interaction with the surface. On the other hand, when 12% WO_3 is mounted on Al_2O_3, the metatungstate anion experiences favorable conditions (low pH) for adsorption onto the positive Al_2O_3 surface. Approximately 10^{20} WO_3 species per gram of Al_2O_3 are added at the sacrifice of Al_2O_3 hydroxyl sites. Thus, the amount of adsorption/exchange originally occurring on Al_2O_3 will likely be decreased. Consequently, although the addition of a favorable adsorption phase (WO_3) would suggest an increase in the adsorption of Co^{2+} onto the composite, we in fact see a decrease. To quantify this hypothesis would require a detailed model for adsorption on composite oxides that included not only surface charge effects but also the number of protonated/deprotonated sites available, as well as the pH-dependent concentration of charged and neutral sites. This is beyond the scope of the present work.

Our modeling of the charge development on composite oxides (*8*) is based on simple additive contribution of each phase (based on surface area) to the measured pzc. Based on this, the WO_3 phase would be "negative" (pH preparation > pzc WO_3) and adsorption should be favorable on this phase. However, the estimated surface area of the second phase is ~15 m^2/g (*8*), which would

suggest that the measured adsorbed amount should be greater than bulk WO_3 but less than Al_2O_3 (surface area ~150 m^2/g). The TPRd results and the results of adsorption from the impregnation solutions cited above suggest that a substantial amount of Co is associated with the dispersed tungsten phase (see, e.g., Table 3).

When this work was initiated, our interests were motivated by demonstrating the selective metal-support exchange concept and its potential effects on the catalytic properties of a metal mounted on a dispersed second phase oxide. An analogue to our system, which could serve as a basis for comparison, namely the $Co/Mo/Al_2O_3$ hydrodesulfurization catalyst, was not considered. This catalyst system has been studied in detail and considerable information on the structure of the catalyst is available (*29*). In the original monolayer model proposed by Schuit and Gates (*30*), it was concluded that most of the Co resided within the alumina. However, Johnson *et al.* (*31*) using a battery of techniques demonstrated that a significant fraction of Co does not and that Co and Mo interact. This was the same conclusion reached by Topsoe and Topsoe (*32*), who showed, using IR spectra of adsorbed NO, that an interaction between Co and Mo exists. Like Mo(VI), W(VI) forms tungstates. Pertinent to this discussion are those structures characterized by WO_6 octahedra. The structure of these crystals is a distorted hexagonal close-packed array of oxide ions with tungsten in octahedral holes; the divalent Co cations are located in two sets of nonequivalent distorted octahedral sites (*33*). There is considerable controversy in the literature as to whether tungsten oxide is octahedrally or tetrahedrally coordinated to the alumina surface (*2, 34*). If the former case exists, it could serve as an anchoring site for Co^{2+} adsorption during catalyst preparation. This cobalt-containing phase would be highly dispersed at low Co weight loading tracking the WO_3 dispersity but could form a contiguous structure in its oxidized state when loadings of 6% are considered. Recall the decrease in particle size for the reduced composite, subsequent to reduction, that we report based on XPS data. Regions of the 76-nm oxidized particles that were not "rich" in a Co^{2+}–W phase could be reduced and they along with the more active Co^{2+}–W would become the catalytic centers for the enhanced activation of CO bond breaking.

CONCLUSIONS

We have demonstrated the concept of selective metal-support exchange in the $Co–WO_3/Al_2O_3$ system. Composite oxides, the pzc's of which lie between the pzc values of the pure phases, appear to provide novel support systems for catalyst design. When a catalytic metal such as cobalt is directed primarily to the dispersed phase of the composite, we find that its resulting catalytic performance is unique.

The higher activity observed for the composite catalyst compared to Co/Al_2O_3 would correlate with formation of a more active species on the composite catalyst. Such species may consist of oxidic and reduced Co^{2+}–W interaction species and possibly some reduced Co_3O_4 that is in contact with these species. We do not favor interpreting the active center as cobalt tungstate. Here, as observed by many, surface compounds can form on oxide catalysts that have no bulk analogues. In this system, we simply have the possibility of forming a more complex inventory of these surface compounds.

ACKNOWLEDGMENTS

This work was supported by NSF under Grant CBT-8900514. The electron microscopy was performed at the electron beam microanalysis facility within the Department of Geology at the University of New Mexico. Reference in this report to any specific commercial product, process, or service is to facilitate understanding and does not necessarily imply its endorsement or favoring by the United States Department of Energy. The authors appreciate the very helpful comments of one of the reviewers of this manuscript.

REFERENCES

1. Ng, K. T., and Hercules, D. M., *J. Phys. Chem.* **80,** 2094 (1976).

2. Salvati, L., Makovsky, L. E., Stencel, J.M., Brown, F. R., and Hercules, D. M., *J. Phys. Chem.* **85,** 3700 (1981).
3. Stencel, J. M., Makovsky, L. E., Diehl, J. R., and Sarkus, T. A., *J. Raman. Spectrosc.* **15,** 282 (1984).
4. Wachs, I. E., Chersich, C. C., and Hardenbergh, J. H., *Appl. Catal.* **13,** 335 (1985).
5. Iannibello, A., Villa, P. L., and Marengo, S., *Gazz. Chim. Ital.* **109,** 5121 (1981).
6. Tittarelli, P., Iannibello, A., and Villa, P. L., *J. Solid State Chem.* **37,** 95 (1981).
7. Grüert, W., Shpiro, E. S., Feldhaus, R., Anders, K., Antoshin, G. V., and Minachev, Kh.M., *J. Catal.* **107,** 522 (1987).
8. Brady, R. L., Southmayd, D., Contescu, C., Zhang, R., and Schwartz, J. A., *Catal.* **129,** 195 (1991).
9. Zhang, R., Jagiello, J., Schwarz, J. A., and Datye, A., *Appl. Catal.* (in press, 1992).
10. Baes, C. F., and Mesmer, R. E., "The Hydrolysis of Cations," p. 238. Wiley, New York, 1976.
11. Reuel, R. C., and Bartholomew, C. H., *J. Catal.* **85,** 63 (1984).
12. Huang, Y.-J., Xue, J., and Schwarz, J. A., *J. Catal.* **111,** 59 (1988).
13. Stranick, M. A., Houalla, M., and Hercules, D. M., *J. Catal.* **103,** 151 (1987).
14. Stranick, M. A., Houalla, M., and Hercules, D. M., *J. Catal.* **125,** 214 (1990).
15. Huang, Y.-J., Schwartz, J. A., Diehl, J. R., and Baltrus, J. P., *Appl. Catal.* **30,** 163 (1988).
16. Press, W. H., Flannery, B. P., Teukolisky, S. A., and Vetterling, W. T., "The Art of Scienfic Computing," p. 155. Cambridge Univ. Press, Cambridge/New York/Port Chester/Melbourne/Sydney, 1989.
17. Chin, R. L., and Hercules, D. M., *J. Phys. Chem.* **86,** 360 (1982).
18. Southmayd, D., Masters thesis, Syracuse University, 1991; and manuscript in preparation.
19. Kadkhodayan, A., and Brenner, A., *J. Catal.* **117,** 311 (1989).
20. Mieth, J. A., and Schwarz, J. A., *J. Catal.* **118,** 203 (1989).
21. Lee, W. H., and Bartholomew, C. H., *J. Catal.* **120,** 256 (1989).
22. See, e.g., Glugla, P. G., Bailey, K. M., and Falconer, J. L., *J. Phys. Chem.* **92,** 4474 (1988); Glugla, P. G., Bailey, K. M., and Falconer, J. L., *J. Catal.* **115,** 24 (1989); Sen, B., and Falconer, J. L., *J. Catal.* **117,** 404 (1989); Sen, B., and Falconer, J. L., *J. Catal.* **133,** 444 (1988).
23. Reuel, R. C., and Bartholomew, C. H., *J. Catal.* **85,** 78 (1984).
24. Fu, L., and Bartholomew, C. H., *J. Catal.* **92,** 376 (1985).
25. Palmer, R. L., and Vroom, D. A., *J. Catal.* **50,** 244 (1977).
26. Ignatiev, A., and Matsuyama, T., *J. Catal.* 58, 328 (1979).
27. Lee, J.-H., Lee, P.-K., and Ihm, S.-K, *J. Catal.* **113,** 544 (1988).
28. Kellner, C. S., and Bell, A. T., *J. Catal.* **75,** 251 (1982).
29. Topsoe, H., Clausen, B. S., Topsoe, N. Y., and Pedersen, E., *Ind. Eng. Chem. Fundam.* **25,** 25 (1986).
30. Schuit, G. C. A., and Gates, B. C., *AIChE J.* **19,** 417 (1973).
31. Johnson, M. F. L., Voss, A. P., Bauer, S. H., and Chiu, N.-S., *J. Catal.* **98,** 51 (1986).
32. Topsoe, N.-Y., and Topsoe, H., *J. Catal.* **75,** 354 (1982).
33. Navrotsky, A., and Kleppa, O. J., *Inorg. Chem.* **8,** 756 (1969).
34. Horsely, J. A., Wachs, I. E., Brown, J. M., Via, G. H., and Hardcastle, F. D., *J. Phys. Chem.* **91,** 4014 (1987).